

Two-step deposition method for high-efficiency perovskite solar cells

Jin-Wook Lee and Nam-Gyu Park

Perovskite solar cells based on organolead halide perovskite light absorbers have been considered a promising photovoltaic technology due to their superb power-conversion efficiency along with cheap material cost. Since the first work on long-term durable solid-state perovskite solar cells, a tremendous volume of research on perovskite solar cells has been carried out. A high photovoltaic performance is mainly attributed to the high-quality $CH_3NH_3PbI_3$ ($MAPbI_3$) material that is strongly dependent on the fabrication method used. $MAPbI_3$ can be prepared by either a single-step procedure or a sequential two-step deposition technique. The two-step method was found, in general, to show better coverage, morphology, and infiltration into a mesoporous oxide layer, which led to high-quality perovskites with desirable optoelectronic properties and thereby high-efficiency perovskite solar cells.

Introduction

A perovskite with a chemical formula of ABX_3 is a crystal structure having corner-sharing octahedral AX_6 and face-sharing cubo-octahedral BX_{12}. The organometal halide RMX_3 (R = methylammonium or foramidnium, M = Pb or Sn, X = Cl, Br, I, or mixed halide) is a key material for perovskite solar cells (see the Introductory article in this issue of *MRS Bulletin*). Three-dimensional (3D) lead and tin methylammonium halides were first reported in 1978,[1,2] where their color changed from colorless to black as the halide would change from chloride to iodide due to a decrease in the bandgap. Layered 2D organotin halides were reported to show an insulator-metal transition when modulating the number of inorganic layers in the $(C_4H_9NH_3)_2(CH_3NH_3)_{n-1}Sn_nI_{3n+1}$ perovskite,[3] which received attention because high-temperature superconducting properties were possible from organic–inorganic perovskite materials.

Contrary to the 2D materials, little attention has been paid to the photovoltaic ability of 3D organic–inorganic halide perovskite materials due to their poor optoelectronic properties. In 2009, the Miyasaka group first used $MAPbI_3$ (MA = CH_3NH_3) as an inorganic sensitizer in dye-sensitized liquid junction-type solar cells,[4] yielding a power-conversion efficiency (PCE) of ~4%. However, this paper was not cited for two years because it reported a much lower PCE as compared with ruthenium-based dyes, which was the most commonly used molecular-type sensitizer in dye-sensitized liquid-type solar cells.

In 2011, Park's group reported a $MAPbI_3$ perovskite-sensitized solar cell with an improved efficiency of 6.5%.[5] Although their report described more advanced technology for higher efficiency through the utilization of a spin-coating method using an optimized precursor solution, this result was not cited until the development of a long-term stable perovskite solar cell in 2012 by Park's group,[6] overcoming the instability of $MAPbI_3$ in a polar liquid electrolyte. Research on perovskite solar cells has been triggered by the discovery of the long-term durable solid-state perovskite solar cell.[6] The number of research papers related to perovskite solar cells has changed from 1 in 2009, 1 in 2011, 4 in 2012, and 56 in 2013, to 460 in 2014.

As a result of subsequent intensive research, the National Renewable Energy Laboratory certified a PCE of 20.1%, fabricated by the Korea Research Institute of Chemical Technology, at the end of 2014.[7] Such a high photovoltaic performance is mainly attributed to high-quality $MAPbI_3$ material, whose quality depends significantly on the fabrication method used. $MAPbI_3$ can be prepared by either a one-step spin-coating procedure or a sequential two-step deposition technique. The morphology and optoelectronic properties were found to be better controlled by a two-step method. In this article, two-step deposition technologies for high-efficiency perovskite solar cells are described in detail.

Jin-Wook Lee, Department of Energy Science, Sungkyunkwan University, South Korea; jw.lee@skku.edu
Nam-Gyu Park, School of Chemical Engineering, Sungkyunkwan University, South Korea; npark@skku.edu
DOI: 10.1557/mrs.2015.166

© 2015 Materials Research Society
https://doi.org/10.1557/mrs.2015.166 Published online by Cambridge University Press

Device structure

Perovskites were initially used as a sensitizer in the dye-sensitized solid-state solar cell structure, in which photogenerated electrons in the perovskite were injected into TiO_2. The balanced electron and hole diffusion lengths observed in $MAPbI_3$[8,9] allow this material to be used in a *p-n* or *p-i-n* junction structure, for which a mesoscopic nanostructure (**Figure 1**a) and a planar structure (Figure 1b) have been studied. Both structures contain a thin compact TiO_2 layer, but the mesoscopic structure possesses a mesoporous oxide layer.

In the mesoscopic structure, sometimes a perovskite capping layer forms on the mesoporous oxide layer. Therefore, in contrast to the planar structure, the mesoscopic structure has two different morphologies: the nanocrystalline perovskite formed in the pores of the oxide film and the bulk perovskite formed in the capping layer. There is no doubt that the perovskite provides electron and hole pathways in the planar structure, whereas electrons can be transported both in the oxide layer and in the perovskite layer for the mesoscopic structure. It should be noted that although the working mechanism might be different depending on the device structure, the photovoltaic performance is mainly dependent on the quality of the perovskite regardless of the device structure.

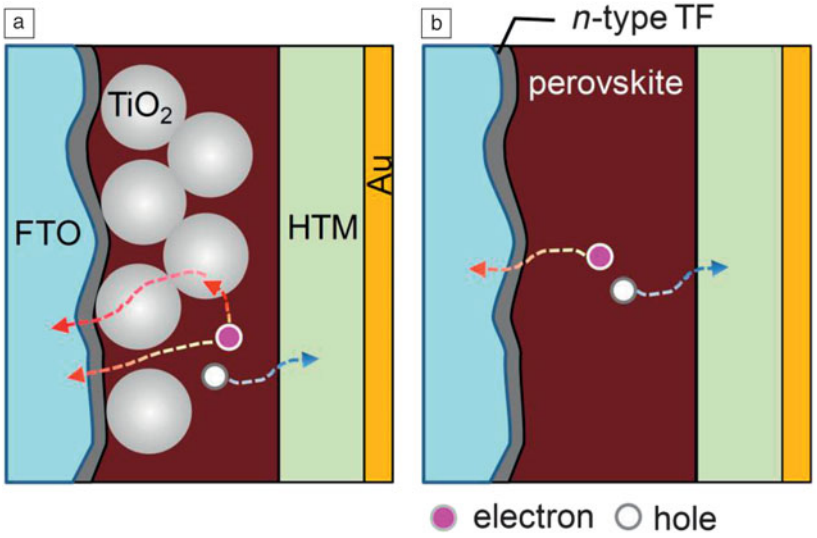


Figure 1. (a) Mesoscopic perovskite solar cell employing a mesoporous TiO_2 layer and (b) planar structure without a mesoporous oxide layer. The thin film (TF) on fluorine-doped tin oxide (FTO) is an electron collecting *n*-type semiconductor. HTM represents hole transporting material. Flows of an electron and a hole are represented by arrows. Reprinted with permission from Reference 10. © 2015 Wiley.

Perovskite fabrication methods

Solution process: One-step versus two-step coating

$MAPbI_3$ can be readily formed by a solution process via a spin-coating technique. Two procedures have been proposed—one-step and two-step deposition methods. For one-step spin-coating, a precursor solution is prepared by mixing MAI (or MACl) and PbI_2 in polar aprotic solvents such as *N*,*N*-dimethylformamide (DMF) or gamma-butyrolactone (GBL).[4–6,11] Spin-coating of the precursor solution is followed by drying and heating at mild temperatures (70°C~170°C), where the spinning rate, drying process, and temperature are expected to affect the $MAPbI_3$ morphology.

Mitzi's group first proposed sequential two-step coating for overcoming difficulties with morphology control and choice of solvent involved with the one-step spin-coating technique in 1988.[12] A PbI_2 film was first deposited on a substrate using vacuum evaporation or spin coating, either of which was followed by dipping in a MAI solution to form $MAPbI_3$. Grätzel's group used this technique for perovskite solar cells, where the dipping time and concentration of the PbI_2 precursor solution were found to affect photovoltaic performance.[13] A modified two-step coating method without the dipping process was proposed, where the PbI_2 solution was first coated on the substrate to form a layered PbI_2 film, and then the 2-propanol solution of CH_3NH_3I was spun

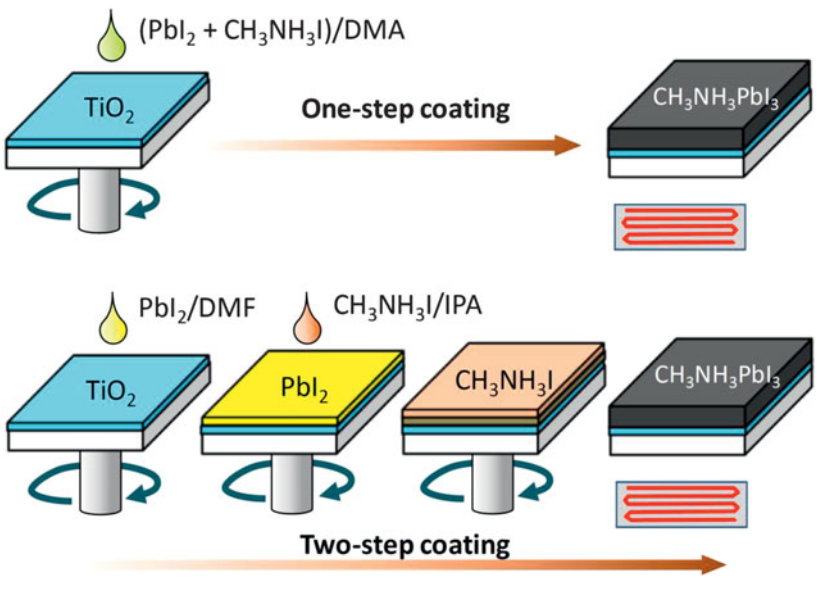


Figure 2. One-step and two-step coating procedures to deposit $MAPbI_3$ perovskite films. The one-step coating procedure was conducted using a single precursor solution containing MAI (CH_3NH_3I) and PbI_2, while the two-step coating method was performed by reacting the spin-coated PbI_2 film with the MAI solution. DMA, DMF, and IPA represent *N*,*N*-dimethylacetamide, *N*,*N*-dimethylformamide, and isopropyl alcohol, respectively. Reprinted with permission from Reference 14. © 2014 AIP Publishing. Note: MA, CH_3NH_3.

https://doi.org/10.1557/mrs.2015.166 Published online by Cambridge University Press

onto the TiO_2 film.[14,15] **Figure 2** shows schematics of the procedures for the one-step and two-step spin-coating methods. In the case of using a single solvent such as DMF or *N*,*N*-dimethylacetamide (DMA), one-step spin coating (average PCE = 7.5%) was found to be inferior to two-step spin coating (average PCE = 13.9%) in terms of photovoltaic performance due to significant differences in the morphology of $MAPbI_3$.[14]

The crystal size of the perovskite can be readily controlled by the two-step spin-coating method. In this procedure, the size of $MAPbI_3$ was found to be significantly altered by the concentration of MAI in the second step of spin coating.[15] Crystal size increased as the MAI concentration decreased, for instance, a 38 mM solution produced 700 nm-sized $MAPbI_3$ crystals, but a 63 mM solution yielded a smaller size of approximately 90 nm, as seen in **Figure 3**. The shape of $MAPbI_3$ crystal was cuboid, irrespective of the MAI concentration.

Besides morphological control by two-step spin coating via MAI concentration change, it is also important to note that photovoltaic performance is strongly influenced by the $MAPbI_3$ size. **Figure 4**a–d compares photovoltaic parameters with respect to the $MAPbI_3$ size.[15] Photocurrent density increased with increasing $MAPbI_3$ size, while the photovoltage was the highest at an intermediate size of about 200 nm. Fill factor generally becomes higher with increasing $MAPbI_3$ size. It was found that the increasing photocurrent with increasing size could be ascribed to the improved light harvesting efficiency, as can be seen in Figure 4e, as well as better charge extraction ability, as confirmed by photo-CELIV (photogeneration and carrier extraction by linearly increasing the voltage) in Figure 4f, in which photo-CELIV measured hole carrier extraction by linearly increasing the voltage under illumination using FTO/bl-Al_2O_3/mp-TiO_2/$MAPbI_3$/spiro-OMeTAD/Au assemblies (FTO = fluorine-doped tin oxide; bl = blocking layer; mp = mesoporous; spiro-OMeTAD = 2,2′,7,7′-tetrakis(*N*,*N*-di-*p*-methoxyphenylamine)-9,9-spirobifluorene). However, considering $\Delta j/j_0$ (Δj = extraction current, j_0 = capacitive displacement current) is proportional to the hole mobility, a slightly lower photovoltage for a crystal size of 700 nm is

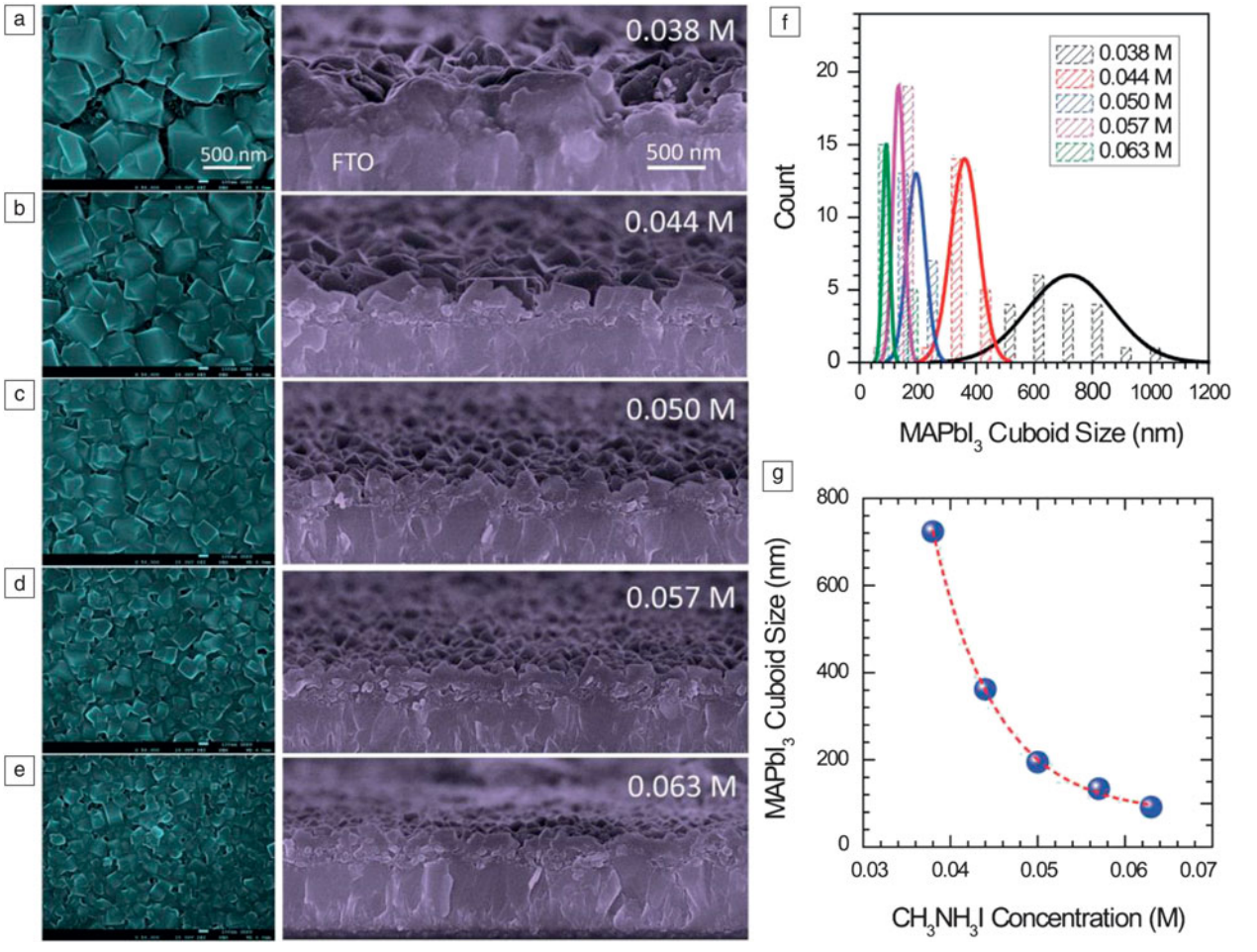


Figure 3. (a–e) Plan-view and cross-sectional scanning electron microscopy images of $MAPbI_3$ crystals, (f) size distribution (solid line indicates Gaussian distribution fitting), and (g) size of $MAPbI_3$ cuboids depend on MAI (CH_3NH_3I) concentration. All the images in the respective columns were taken at the same magnification. The size of the $MAPbI_3$ cuboid crystal increases for decreasing MAI concentration. Reprinted with permission from Reference 15. © 2014 Nature Publishing Group. Note: MA, CH_3NH_3; FTO, fluorine-doped tin oxide.

https://doi.org/10.1557/mrs.2015.166 Published online by Cambridge University Press

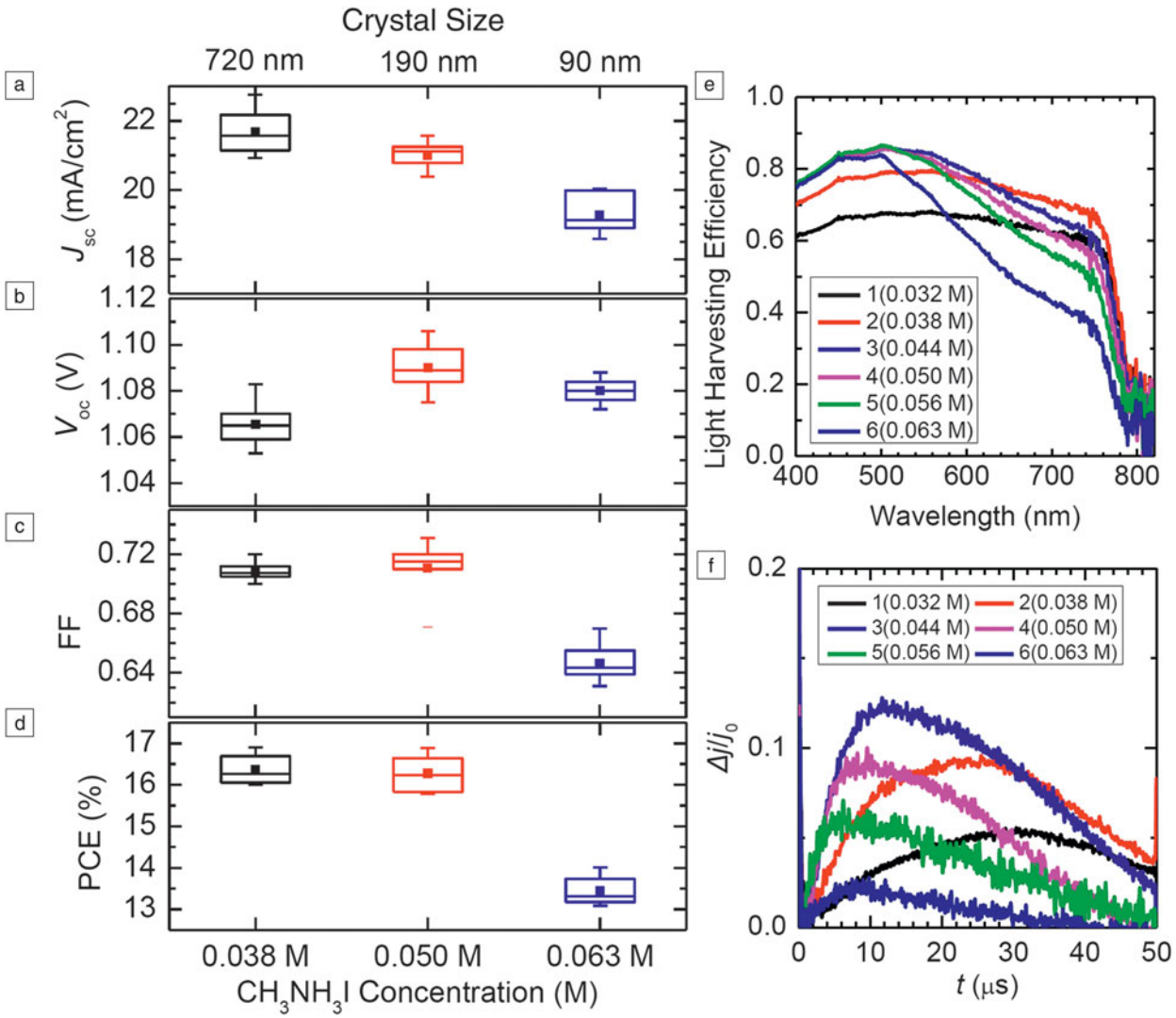


Figure 4. Effect of MAI (CH_3NH_3I) concentration on (a) short-circuit current density (J_{sc}), (b) open-circuit voltage (V_{oc}), (c) fill factor (FF), (d) power-conversion efficiency (PCE), (e) light harvesting efficiency, and (f) photo-CELIV (charge extraction by linearly increasing voltage) transients. For each data point, the bottoms and tops of boxes indicate first and third quartiles, respectively. The PCE increases with decreasing MAI concentration. Light harvesting efficiency increases with decreasing MAI concentration until 0.032 M, while charge extraction becomes faster with increasing MAI concentration. In photo-CELIV spectra, the rise time of the $\Delta j/j_0$ curve is inversely proportional to the charge extraction rate, and the area under the curve corresponds to the total amount of extracted charge. The device configuration was FTO/bl-TiO_2/mp-TiO_2/$MAPbI_3$/spiro-OMeTAD/Au for *J–V* measurements and FTO/bl-Al_2O_3/mp-TiO_2/$MAPbI_3$/spiro-OMeTAD/Au for the photo-CELIV study. Reprinted with permission from Reference 15. © 2014 Nature Publishing Group. Note: MA, CH_3NH_3; *t*, time; Δj, extraction current; j_0, capacitive displacement current; FTO, fluorine-doped tin oxide; bl, blocking layer; mp, mesoporous; spiro-OMeTAD, 2,2′,7,7′-tetrakis(*N*,*N*-di-*p*-methoxyphenylamine)-9,9-spirobifluorene.

probably related to retarded hole mobility compared to the smaller crystals, as can be seen in Figure 4f, because slow hole mobility is likely to increase recombination. To attain high photovoltage along with high photocurrent and fill factor, it is necessary to manipulate the crystal size to yield fast mobility in order to minimize recombination and high charge extraction and light scattering to maximize the photocurrent.

Vacuum process

Perovskite films can also be prepared by the thermal evaporation method. Co-evaporation of MAI and $PbCl_2$ led to a $MAPbI_3$ phase, and uniformity of the film was much better than the solution-processed film.[16] Since vacuum deposition uses two chemical sources, it can be regarded as a two-step coating process in a sense. Thus, MAI can be also deposited onto the PbI_2 film by evaporation.

A vapor-assisted solution process was proposed to grow perovskite films via the *in situ* reaction of an as-deposited film of PbI_2 with MAI.[17] The perovskite film prepared by this method showed a well-defined grain structure with grain size up to the microscale, full surface coverage, and small surface roughness. A sequential two-step vacuum deposition

https://doi.org/10.1557/mrs.2015.166 Published online by Cambridge University Press

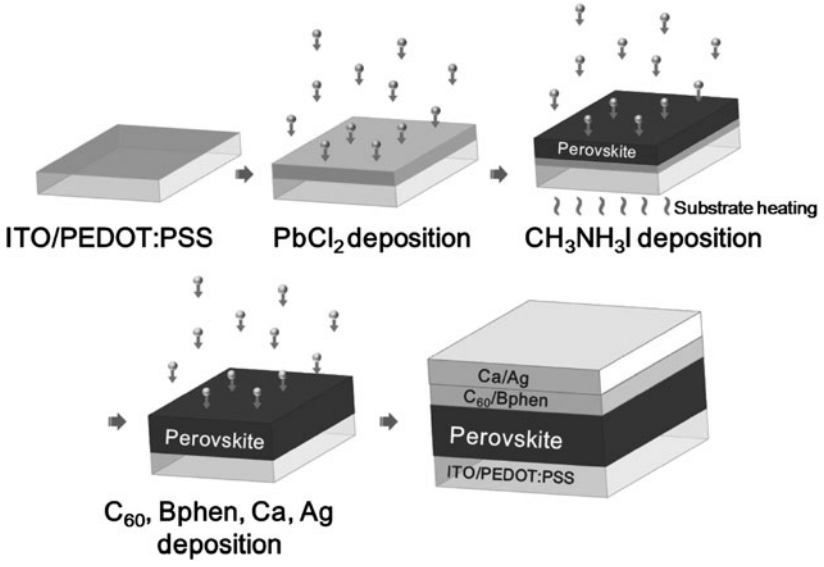


Figure 5. Sequential two-step vacuum deposition using $PbCl_2$ and MAI to fabricate a planar-structured perovskite solar cell. MAI (CH_3NH_3I) was evaporated onto a pre-evaporated $PbCl_2$ film while the substrate was heated. Reprinted with permission from Reference 18. © 2014 Wiley. Note: ITO, indium tin oxide; PEDOT:PSS, poly(3,4-ethylenedioxythiophene):poly(styrene sulfonate); Bphen, Bathophenanthroline; MA, CH_3NH_3.

method (**Figure 5**) was applied to prepare planar structured perovskite solar cells,[18] where MAI was evaporated after $PbCl_2$ evaporation onto an indium-doped tin oxide/poly(3,4-ethylenedioxythiophene) poly(styrene sulfonate) (ITO/PEDOT:PSS) substrate. In this process, the substrate was heated while depositing MAI vapor, and the substrate temperature was found to be critical for photovoltaic performance. For example, photovoltaic performance was better when the substrate was heated to 75°C compared to a substrate temperature of 65°C or 85°C.

Two-step deposition of $HC(NH_2)_2PbI_3$ ($FAPbI_3$)

Although $MAPbI_3$ exhibits superb photovoltaic performance, there are issues to be addressed, including the tetragonal–cubic phase transition at approximately 56°C.[19] This temperature is critical when taking into consideration the solar cell operates at temperatures up to 85°C. The band structure of $MAPbI_3$ can be affected by the phase transition, which also has a negative influence on photovoltaic performance. $HC(NH_2)_2PbI_3$ ($FAPbI_3$) is an alternative to $MAPbI_3$ because $FAPbI_3$ is free from such a phase transition. $FAPbI_3$ can be formed by a two-step deposition process, where the spin-coated PbI_2 film is dipped in a $HC(NH_2)_2I$ (FAI) solution, followed by a heat treatment at 150°C.[20] Similarly, $FAPbI_3$ crystals were fabricated by a two-step deposition procedure, where the morphology was less influenced by the substrate. **Figure 6** shows a similar $FAPbI_3$ morphology regardless of the substrate type: with and without a compact TiO_2 film.

Fabricating an ultrathin layer of $MAPbI_3$ on a $FAPbI_3$ surface (**Figure 7**a) compensates for pin holes formed on the $FAPbI_3$ film surface and additionally increases the incident photon-to-electron conversion efficiency (or incident photon-to-current conversion efficiency) at the optical bandgap absorption, as indicated by the black arrow in Figure 7b. $FAPbI_3$ formed by two-step deposition demonstrates a PCE of 16% and shows better photostability compared to two-step spin-coated $MAPbI_3$.

Summary

A two-step deposition procedure was described to fabricate a $RPbI_3$ ($R = CH_3NH_3$ or $HC(NH_2)_2$) perovskite layer on a substrate with and without a mesoporous TiO_2 film. $MAPbI_3$ could be formed by either dipping or spin coating the PbI_2 film, where crystal size was controlled by varying the MAI concentration. The $MAPbI_3$ crystal size significantly influenced photovoltaic performance. Instead of using the MAI solution, MAI could be evaporated onto the PbI_2 film to form $MAPbI_3$, which is expected to regulate $MAPbI_3$ layer thickness and surface roughness. The evaporation method will be more beneficial for a tandem architecture. Although high photovoltaic performance was realized by the two-step spin-coating method, further efforts need to be devoted to developing a facile method for large-area coating to help facilitate scaling up the process.

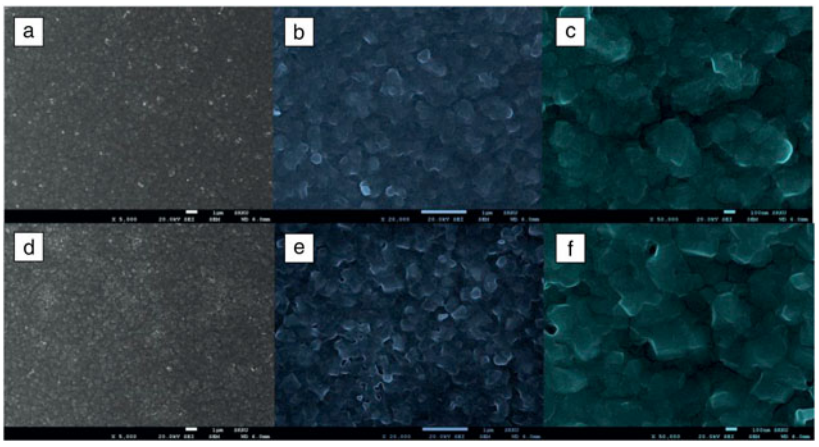


Figure 6. Plan-view scanning electron microscopy images of $FAPbI_3$ coated on (a–c) the compact TiO_2 layer (planar structure without mesoporous TiO_2 layer) and (d–f) the mesoporous TiO_2 layer (mesoscopic structure). The scale bars on left, middle, and right images represent 1 μm, 1 μm, and 100 nm, respectively. Reprinted with permission from Reference 20. © 2014 Wiley. Note: FA, $HC(NH_2)_2$.

https://doi.org/10.1557/mrs.2015.166 Published online by Cambridge University Press

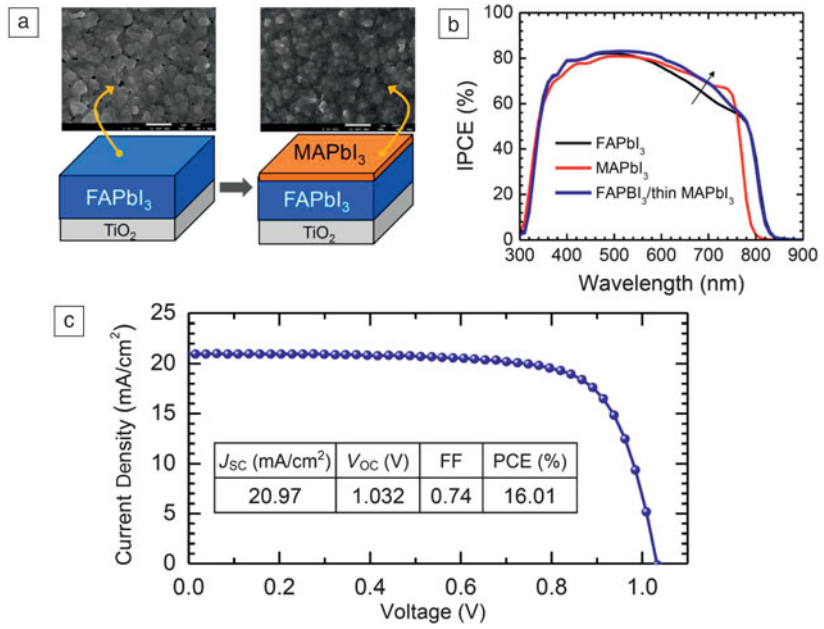


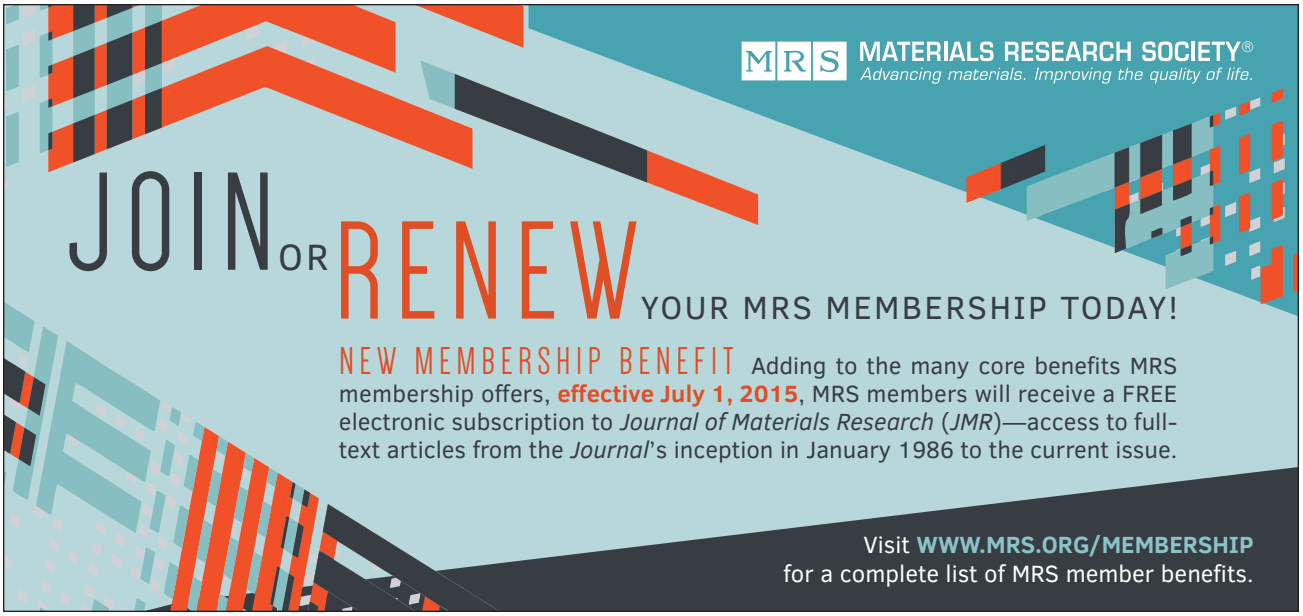
Figure 7. (a) Plan-view scanning electron microscopy images of the $FAPbI_3$ layer with and without the ultrathin $MAPbI_3$ layer. Scale bars indicate 1 μm. (b) Incident photon-to-electron efficiency (IPCE) spectra of perovskite solar cells based on $FAPbI_3$, $MAPbI_3$, and $FAPbI_3$ with thin $MAPbI_3$, where the integrated J_{sc} was calculated to be 19.57, 18.90, and 20.22 mA/cm², respectively. (c) Current–voltage curve of the best performance $FAPbI_3$ perovskite solar cell. J_{SC} improved due to increased band-edge absorption after formation of a thin $MAPbI_3$ layer on top of $FAPbI_3$, as indicated by the black arrow in (b), which resulted in a PCE of 16.01%. Reprinted with permission from Reference 20. © 2014 Wiley. Note: FA, $HC(NH_2)_2$; MA, CH_3NH_3; FF, fill factor; J_{sc}, short-circuit current density; V_{oc}, open-circuit voltage; PCE, power-conversion efficiency.

Acknowledgments

This work was supported by National Research Foundation (NRF) of Korea grants funded by the Ministry of Science, ICT & Future Planning (MSIP) of Korea under contracts No. NRF-2012M1A2A2671721, 2012M3A7B4049986 (Nano Material Technology Development Program), and NRF-2012M3A6A7054861 (Global Frontier R&D Program on Center for Multiscale Energy System).

References

1. D. Weber, *Z. Naturforsch. B: J. Chem. Sci.* **33b**, 1443 (1978).
2. D. Weber, *Z. Naturforsch. B: J. Chem. Sci.* **33b**, 862 (1978).
3. D.B. Mitzi, C.A. Feild, W.T.A. Harrison, A.M. Guloy, *Nature* **369**, 467 (1994).
4. A. Kojima, K. Teshima, Y. Shirai, T. Miyasaka, *J. Am. Chem. Soc.* **131**, 6050 (2009).
5. J.-H. Im, C.-R. Lee, J.-W. Lee, S.-W. Park, N.-G. Park, *Nanoscale* **3**, 4088 (2011).
6. H.-S. Kim, C.-R. Lee, J.-H. Im, K.-B. Lee, T. Moehl, A. Marchioro, S.-J. Moon, R. Humphry-Baker, J.-H. Yum, J.E. Moser, M. Grätzel, N.-G. Park, *Sci. Rep.* **2**, 591 (2012).
7. National Renewable Energy Laboratory, *Best Research-Cell Efficiencies*; http://www.nrel.gov/ncpv/images/efficiency_chart.jpg.
8. G. Xing, N. Mathews, S. Sun, S.S. Lim, Y.M. Lam, M. Grätzel, S. Mhaisalkar, T.C. Sum, *Science* **342**, 344 (2013).
9. S.D. Stranks, G.E. Eperon, G. Grancini, C. Menelaou, M.J.P. Alcocer, T. Leijtens, L.M. Herz, A. Petrozza, H.J. Snaith, *Science* **342**, 341 (2013).
10. H.S. Jung, N.-G. Park, *Small* **11**, 10 (2015).
11. M.M. Lee, J. Teuscher, T. Miyasaka, T.N. Murakami, H.J. Snaith, *Science* **338**, 643 (2012).
12. K. Liang, D.B. Mitzi, M.T. Prikas, *Chem. Mater.* **10**, 403 (1998).
13. J. Burschka, N. Pellet, S.-J. Moon, R. Humphry-Baker, P. Gao, M.K. Nazeeruddin, M. Grätzel, *Nature* **499**, 316 (2013).
14. J.-H. Im, H.-S. Kim, N.-G. Park, *APL Mater.* **2**, 081510 (2014).
15. J.-H. Im, I.-H. Jang, N. Pellet, M. Grätzel, N.-G. Park, *Nat. Nanotechnol.* **9**, 927 (2014).
16. M. Liu, M.B. Johnston, H.J. Snaith, *Nature* **501**, 395 (2013).
17. Q. Chen, H. Zhou, Z. Hong, S. Luo, H.-S. Duan, H.-H. Wang, Y. Liu, G. Li, Y. Yang, *J. Am. Chem. Soc.* **136**, 622 (2014).
18. C.-W. Chen, H.-W. Kang, S.-Y. Hsiao, P.-F. Yang, K.-M. Chiang, H.-W. Lin, *Adv. Mater.* **26**, 6647 (2014).
19. T. Baikie, Y. Fang, J.M. Kadro, M. Schreyer, F. Wei, S.G. Mhaisalkar, M. Grätzel, T.J. White, *J. Mater. Chem. A* **1**, 5628 (2013).
20. J.-W. Lee, D.-J. Seol, A.-N. Cho, N.-G. Park, *Adv. Mater.* **26**, 4991 (2014). □



https://doi.org/10.1557/mrs.2015.166 Published online by Cambridge University Press